MICHIGAN STATE UNIVERSITY

CYCLOTRON LABORATORY

HIGH-SPIN STRUCTURE OF ODD-ODD ^{116}Sb AND ^{118}Sb

W.H. BENTLEY, R.A. WARNER, Wm.C. McHARRIS, and W.H. KELLY

DECEMBER 16, 1985

MSUCL-541

December 16, 1985
MSUCL-541

HIGH-SPIN STRUCTURE OF ODD-ODD ^{116}Sb AND ^{118}Sb

W. H. Bentley,* R. A. Warner,† and Wm. C. McHarris

National Superconducting Cyclotron Laboratory

and

Departments of Physics & Astronomy and of Chemistry

Michigan State University

East Lansing, Michigan 48824

and

W. H. Kelly

Department of Physics

and

College of Sciences and Humanities

Iowa State University

Ames, Iowa 50011

*Present Address: Burroughs Corporation, Coral Springs, Fla. 33065

†Present Address: Battelle Pacific Northwest Laboratories, Richland, Wash. 99352

Abstract:

We have obtained structure information on odd-odd ^{116}Sb and ^{118}Sb by in-beam γ-ray spectroscopy following p-, α-, and ^{7}Li-induced fusion/evaporation reactions. Experiments included γ-ray excitation functions, γ-γ coincidences, angular distributions, and half-life measurements. High-spin level schemes showing remarkably parallel behavior were constructed. Structures of the states are discussed in terms of simple odd-odd (two-particle) states, particles-plus-core states, and deformed rotational bands.

Keyword Abstract:

NUCLEAR REACTIONS $^{115}In(\alpha,3n\gamma)^{116}Sb$, E_α = 37-45 MeV; $^{114}Cd(^7Li,3n\gamma)^{118}Sb$, $E_{^7Li}$ = 22-30 MeV; $^{120}Sn(p,3n\gamma)^{118}Sb$, E_p = 30 MeV; measured E_γ, I_γ, γ-γ coinc., $\sigma(\theta)$, $\sigma(E)$, $t_{1/2}$(γ-γ-t coinc.); deduced ^{116}Sb, ^{118}Sb levels, J, π; enriched and natural targets, Ge and Ge(Li) detectors; shell and collective model structures.

PAC Numbers: 25.90+k, 25.40.Jt, 21.60.Ev, 21.60.Cs

I. INTRODUCTION

The detailed nuclear structure of many of the odd-odd Sb isotopes has been the subject of extensive and varied recent investigations. These have included the isotopes: ^{112}Sb (Refs. 1,2), ^{114}Sb (Ref. 1,3,4), ^{116}Sb (Refs. 1,3-6), ^{118}Sb (Refs. 7-9), ^{120}Sb (Refs. 7,10-11), and ^{122}Sb (Refs. 10,12). Most of these studies, however, have concentrated on the spherical, low-lying, low-spin states in these nuclei, the exceptions being the high-spin studies of Refs. 3,4, and 8. There have also been a number of comprehensive investigations[12-15] of the odd-mass Sb nuclei, which have included the study of high-spin states, providing information on deformed states which coexist with the spherical states in these nuclei. Similarly deformed states are expected to exist in the high-spin level structure of odd-odd Sb nuclei. In order to determine if such states do indeed exist, it is desirable to extend the experimental knowledge of these nuclei to high-spin states. This paper reports on our experimetnal investigations of the high-spin states in ^{116}Sb and ^{118}Sb.

We have obtained information concerning the level structures of ^{116}Sb and ^{118}Sb by observing γ-rays produced following p-, α-, and ^{7}Li-induced fusion/evaporation reactions. Experiments included γ-ray excitation functions, γ-γ coincidences, γ-ray angular distributions, and half-life measurements. Level schemes were determined for both nuclei and were found to display remarkably similar behavior. For example, included in each of the level schemes are two bands each built on J = 7 states. As will be discussed, these bands can be qualitatively described with a two-particle-plus-rotating-core model, thus providing evidence supporting the coexistence of deformed states in odd-odd Sb nuclei.

II. EXPERIMENTAL TECHNIQUES AND RESULTS

A. Targets and Reactions

High-spin states in ^{116}Sb were populated primarily by the ^{115}In(α,3nγ) reacion. The α beams (37-45 MeV) were produced by the Michigan State University 50-MeV Cyclotron. The target was a natural In foil of about 1 mg/cm^2 thickness. (^{115}In has a natural isotopic abundance of 95.7%.) The predominant competing reactions are (α,2nγ) and (α,4nγ), which produced the neighboring odd-mass Sb isotopes. Additional transitions result from the β decay of the Sb nuclei to the corresponding Sn nuclei. Since the present results contain no new information with respect to these other nuclei, no further reference is made to these transitions except to indicate where they interfere with the results for ^{116}Sb.

High-spin states in ^{118}Sb were populated primarily by the ^{114}Cd(^{7}Li,3nγ) reaction. The ^{7}Li beams (22-30 MeV) were produced by the Notre Dame University Tandem Van de Graaff Accelerator. The target was a self-supporting metallic foil enriched to 96% in ^{114}Cd (obtained from Oak Ridge National Laboratory) having a thickness of approximately 1 mg/cm^2. In this case competing reactions included 2n and 4n evaporation to neighboring odd-mass Sb nuclei, as well as charged particle evaporation to ^{115}In, ^{116}In, and ^{115}Cd. Additional transitions result from the β decay of the In and Sb nuclei to the corresponding Sn nuclei. As with the case of the ^{116}Sb experiments, no new information was obtained regarding these other nuclei; consequently, no further reference is made to these transitions except to indicate where they interfere with the results for ^{118}Sb.

Additional experiments were performed for ^{118}Sb using the ^{120}Sn(p,3nγ) reaction. The p beams (30 MeV) were produced by the Michigan State University Cyclotron. The target was a self-supporting metallic foil of 0.5 mg/cm^2 thickness, isotopically enriched to 98% in ^{120}Sn (obtained from Oak Ridge National Laboratory). This reaction was much more selective in producing the ^{118}Sb isotope. As a result, these spectra contain many fewer peaks than those produced by the ^{7}Li reaction, diminishing the difficulties caused by multiplets. However, in so doing, only levels with spin up to about 11 ħ were populated by this reaction.

The results reported here are limited to high-spin states. These are somewhat arbitrarily taken as those states which decay through the $J^\pi = 8^-$ metastable state, which is known to exist in many of the odd-odd Sb nuclei in this region. Low-spin states which depopulate to the ground state have been extensively studied using the (p,nγ) reaction,[1,5] and thus will not be included here.

B. Angular Distributions

An angular-distribution experiment was performed for ^{116}Sb using an α beam energy of 42 MeV. Relative intensities were measured at eight angles between 90° and 155°. The angles were taken in random order and data were typically collected for two hours. During these measurements an additional surface barrier detector was used to normalize the γ-ray yields at different angles.

For each energy the γ-ray yields were fitted as a function of angle to the usual expression,

$$W(\theta) = A_0 + A_2P_2(\cos\theta) + A_4P_4(\cos\theta),$$

where P_2 and P_4 are Legendre polynomials. The angular distribution coefficients, A_2/A_0 and A_4/A_0 are given in Table I. Transitions for which angular distribution coefficients are not listed are either very weak or are components of closely spaced multiplets, which consequently contained large errors. Where the fitted value of A_4/A_0 displayed a very large uncertainty, the data were refitted with the value for A_4/A_0 constrained to be 0. Also included in this table are the integrated relative intensities. These have been corrected for detector efficiency and were normalized such that the 1399-keV transition has the value 100. A singles spectrum obtained during this experiment at a detector angle of 130° is shown in Fig. 1. Some representative angular distributions, together with their fits are shown in Fig. 2.

The angular-distribution experiment for ^{118}Sb was performed using the (p,3nγ) reaction with a beam energy of 30-MeV. Two sets of measurements

were made, one with a high-resolution, small-volume planar Ge(Li) detector, and the other with a 9%-efficient coaxial Ge(Li) detector. In each of the measurements data were collected at nine angles between 90° and 160°. In the first set x-rays were used to normalize the γ-ray yields at different angles. In the second set an additional fixed Ge(Li) detector was used. These data were treated in the same manner as for ^{116}Sb. Results are given in Table II. For γ-ray energies less than 300 keV the values are taken from the first set of experiments. For energies above 300 keV, they are taken from the second set. Figure 3 shows a singles spectrum obtained during the second set at a detector angle of 125°.

C. γ-γ-t Coincidence Measurements

The γ-γ coincidence experiments formed the basis from which the level schemes were constructed. The ^{116}Sb experiments were performed using an α beam energy of 38 MeV. Two coaxial Ge(Li) detectors, each with an efficiency of approximately 9%, were placed at ±90° with respect to the beam direction. Approximately 30×10^6 coincident events were recorded event-by-event on magnetic tape for off-line sorting with background subtraction.

The γ-γ coincidence experiments for ^{118}Sb was performed using a ^{7}Li beam energy of 26 MeV. Two coaxial Ge(Li) detectors were placed at opposite sides of the target at angles of 90° and 125° with respect to the beam direction. Approximately 20×10^6 coincidence events were recorded. The results of the γ-γ coincidence measurements are listed in Tables III and IV for ^{116}Sb and ^{118}Sb, respectively.

D. Timing Measurements

Pulsed beam γ-ray timing experiments were performed for both ^{116}Sb and ^{118}Sb to measure half-lives of isomeric states. The cyclotron rf signal was used to reference the beam bursts. The data were placed into one of ten spectra depending on the value of the time parameter. These were analyzed off-line.

The measurements for ^{116}Sb were performed using an α beam energy of 38 MeV and an planar intrinsic Ge detector positioned at 90° with respect to the beam direction. Half-lives were determined for 13 γ-rays involved in the decay of six isomeric levels. A summary of these results is given in Table V.

The measurements for ^{118}Sb were performed using a p beam energy of 30 MeV and a planar Ge(Li) detector was positioned at 90° with respect to the beam direction. Half-lives were obtained for two transitions associated with the decay of one isomeric level. A summary of these results is also included in Table V.

E. γ-Ray Excitation Functions

Excitation functions were determined for ^{118}Sb using the ^{7}Li-induced reaction. The intensity of each γ-ray was measured as a function of excitation energy from 22 to 30 MeV, using an 8%-efficient coaxial Ge(Li) detector placed at 125° with respect to the beam direction. Results for several of the more intense transitions are shown in Fig. 4. The intensities have been first normalized to the 318-keV transition and then to this intensity from the 22-MeV reaction. The spectrum obtained from the 28-MeV reaction is shown in Fig. 5, where it can be compared with the spectrum from the p-induced reaction (Fig. 3).

An excitation function was also performed for ^{116}Sb, using the ^{119}Sn(p,4nγ) reaction at 37.8, 40.0, and 44.0 MeV. In these measurements intermediate spin levels up to about 11 ħ were excited.

III. THE ^{116}Sb AND ^{118}Sb LEVEL SCHEMES

A. Level-Scheme Construction

Coincidence information, intensity balances, and excitation functions for individual γ-rays were the primary factors used to construct the level schemes. Spin assignments were made on the basis of angular-distribution coefficients and the excitation-function results. The resulting level schemes for ^{116}Sb and ^{118}Sb are shown in Figs. 6 and 7, respectively.

Each of the high-spin level schemes is built on a $J^{\pi} = 8^{-}$ excited state that deexcites via β^{+} decay to the appropriate Sn nucleus. Because none of the high-spin levels demonstrates observable decay intensity to states decaying to the ground state, we could not determine the excitation energy of these 8^{-} metastable states in this study. The energies used for these levels were adopted from the results of previous studies [212 ± 8 keV for ^{116}Sb (Ref. 17) and 225 ± 60keV for ^{118}Sb (Ref. 1)]. Since all of the level energies assigned in the present study depend on the energies of the 8^{-} states, the relatively large uncertainties associated with these excitation-energy values are transmitted to the excitation energies determined here. Similarly, the spin assignments for these levels, upon which all spin assignments to higher-lying levels depend, are taken from the literature, although these were well-established from atomic beams measurements.[18]

It is evident from the level schemes that the two nuclei display a remarkable amount of similarity, with the most predominant level structures being common to both. Because of this high degree of similarity, the spin assignments for both will be discussed simultaneously. For convenience this

discussion will be divided into four sections, corresponding to the four distinct groups of transitions evident in the level schemes.

B. High-Spin Sequences

This section is devoted to the group of states and transitions shown left-most in the level schemes. They carry a large amount of the decay intensity from high-excitation energies, indicating that the states in this group are yrast or near-yrast states. This suggestion is also supported by the excitation function data for these transitions. The comparatively steep slopes displayed by these transitions indicate high-spin levels. For these reasons this sequence of transitions is assigned spin values that increase with energy.

The first state lies at 978 keV in ^{116}Sb and at 892 keV in ^{118}Sb. Each decays by an intense, predominantly dipole transition, as determined from the angular distribution data, to the respective 8^- isomeric state. Consequently, J = 9 is assigned to these two states. A significant quadrupole component for the transition in ^{116}Sb indicates it to be M1 + E2, establishing the parity as negative. A tentative assignment of negative parity is also made for the corresponding state at 892 keV in ^{118}Sb from these systematics.

The state at 1379 keV in ^{118}Sb has no easily observable counterpart in ^{116}Sb. We assigned it J = 9 based on the $\Delta J = 1$ angular distribution behavior of the 1167-keV transition which depopulates it.

The states at 1603 keV in ^{116}Sb and 1533 keV in ^{118}Sb are each depopulated by two transitions, a very intense E2 transition to the 8^- state and a much weaker mixed M1/E2 transition to the previously discussed 9^- state. This is consistent with a 10^- assignment for each.

The state at 1685 keV in ^{118}Sb has no easily observable counterpart in ^{116}Sb. It is tentatively assigned J = 10. This is based on

the excitation-function results for the three transitions which depopulate it. They display behavior parallel to that of the 1321-keV transition which depopulates the better-established 10^- state.

The states at 1624 keV in ^{116}Sb and 1695 keV in ^{118}Sb, although counterparts, depopulate by somewhat different paths. The 1695-keV state in ^{118}Sb decays only to the 10^- level via an intense, prompt 161-keV transition, which displays the angular-distribution characteristics of a stretched $\Delta J = 1$ transition, thus suggesting a $J = 11$ assignment for the 1695-keV state. On the other hand, the 1624-keV level in ^{116}Sb depopulates not only to the 10^- 1603 keV state, but also to the 9^- and 8^- states. The transition to the 1603-keV state has an energy of only 22 keV, too small to be observed in any of our experiments. Its existence was determined by a 4.1-nsec delayed component in the 1378-keV transition. Its energy was estimated from the difference in level energies, and its intensity was estimated from the ratio of the 1378- and 1399-keV transitions in a delayed-coincidence spectrum.

The 1399-keV transition which depopulates the 1624-keV state is the most intense transition in the ^{116}Sb level scheme. It has an angular distribution with a very large positive A_2 value ($A_2 = 0.53$, $A_4 \approx 0$). This angular-distribution result, along with the 4.1-nsec half-life measurement for the 1624-keV state, suggests the multipolarity of this transition to be E3. The 647-keV transition has an angular distribution consistent with a slightly mixed M2 + E3 transition. Therefore, we assign 11^+ to the 1624-keV state. We then make a tentative parallel assignment (with positive parity) for the corresponding 1695-keV state in ^{118}Sb.

We can make definite assignments for only three additional states in the "high-spin sequences." These are the states at 2808, 3049, and 3275

keV in ^{116}Sb. The 2808-keV state depopulates via a 1184-keV transition displaying E2 characteristics in its angular distribution. Consequently, we assign 13^+ to the 2808-keV state. The E2 angular-distribution behavior of the 467-keV transition and the mixed M1 + E2 behavior of the 226- and 241-keV transitions allow us to assign the 3049- and 3275-keV states 14^+ and 15^+, respectively. It is tempting to make parallel assignments for the corresponding states in ^{118}Sb, but actually there are insufficient data for making assignments for these states or for any other states involved in the high-spin sequences. All we can say is that these unassigned states undoubtedly have $J \geq 13$.

C. The Lower-Lying J = 7 Bands

Displayed to the immediate right of the high-spin sequence in each of the level schemes is what appears to be a rotational band built on a J = 7 state. This state lies at 1001 keV in ^{116}Sb with a half-life of 12.6 nsec and at 927 keV in ^{118}Sb with a half-life of 21.7 nsec. The band is much better established in ^{118}Sb, where it is populated more strongly than in ^{116}Sb. If one purposely uses the over-simplified rotational-energy equation,

$$E_J = E_0 + \frac{\hbar^2}{2\mathcal{J}} J(J+1),$$

he finds $\hbar^2/2\mathcal{J}$ to be 25.7 keV for the band in ^{116}Sb and 23.2 keV for the band in ^{118}Sb. The respective errors in generating the 9^+ state are 7% and 5%, not bad for a high-spin rotational band even in well-deformed nuclear regions.

In ^{116}Sb all of the proposed $\Delta J = 1$ stopover band transitions are weak components of closely spaced multiplets, causing difficulties in the extraction of accurate energies, intensities, and angular distribution coefficients. Because of this the 435-keV transition is only tentatively placed as the highest member in this sequence. Uncertainties in the intensities of the 424- and 405-keV transitions make the ordering of these two transitions ambiguous. The order was chosen as shown in the figure to accommodate the placement of the two tentatively placed crossover transitions. It should be noted there is no evidence for a $9 \rightarrow 7$ crossover transition.

In each of the two nuclei the band heads depopulate in the same manner. The spin assignments are based on $\Delta J = 1$ transitions (776 keV in ^{116}Sb and 715 keV in ^{118}Sb) to the respective 8^- metastable states. This limits the possible spin values to 7 or 9. The excitation-function results for these transitions then establish $J = 7$ assignment as the correct alternative. Each one also depopulates to a $J = 7$ state. These transitions (350 keV in ^{116}Sb and 397 keV in ^{118}Sb) have angular distributions consistent with $\Delta J = 0$, $7 \rightarrow 7$ transitions.

The band members are assigned spin values increasing by $\Delta J = 1$ with energy, based on the angular-distribution behavior of the cascade transitions, all consistent with M1/E2, $\Delta J = 1$ transitions having positive mixing ratios. In Section IV.B we discuss these bands in terms of the rotational model. This model suggests a configuration with positive parity. However, because there is no model-independent experimental evidence supporting positive parity assignments for these bands, we leave it as only a tentative suggestion.

D. The Higher-Lying J = 7 Bands

Displayed immediately to the right of the J = 7 band on each level scheme is what could be another rotational band with J = 7. The band head lies at 1193 keV in ^{116}Sb and at 1149 keV in ^{118}Sb. The members of these "rotational bands" are not nearly so well-ordered as those of the previously discussed J = 7 rotational bands. In fact, at first glance it would appear that "better" rotational bands having J = 8 could be constructed based on the states at 1293 in ^{116}Sb and 1186 keV in ^{118}Sb. However, the γ-ray transitions probabilities show that the J = 7 states are very closely related to the J = 8 states, and in Section IV.B we shall show how these J = 7 bands can be explained in terms of decoupled odd-proton and odd-neutron states.

The 1193- and 1149-keV states are assigned J = 7, based on $\Delta J = 1$ transitions (968 keV in ^{116}Sb and 937 keV in ^{118}Sb) to the respective 8^- metastable states. The excitation functions are also consistent with such assignments. Additional confirmation comes from the $\Delta J = 1$ transitions (1283 keV in ^{116}Sb and 1177 keV in ^{118}Sb) from the J = 9 band members.

In ^{118}Sb the $8 \rightarrow 7$ transition has only 37 keV of energy, too low to be observed in our experiments. Its existence was established by the 1177-keV transition from the J = 9 state. However, the ordering of the 203- and 37-keV transitions cannot be made unambiguously. It was chosen as indicated in order to be parallel with the corresponding transitions in ^{116}Sb.

The band members are assigned spin values increasing by $\Delta J = 1$ with energy, based upon the mixed M1 + E2 behavior of the angular distributions of the cascade transitions. In addition, E2 crossover

transitions appear in ^{116}Sb. As with the lower-lying J = 7 bands, no definite parity assignments can be made from the experimental data alone. We shall see in Section IV.B that possible configurations for these bands suggest the parity should be negative.

E. Other States

A few additional spin assignments could be made. Among these are $J = 7$ assignments for the 651-keV state in ^{116}Sb and the 530-keV state in ^{118}Sb. They both deexcite by intense $\Delta J = 1$ transitions to the 8^- metastable state. The excitation functions for these two transitions are not so steep as would be expected for transitions coming from $J = 9$ states, thus favoring the lower-spin alternatives.

We assign $J = 8$ for the 523-keV state in ^{116}Sb on the basis of the $\Delta J = 1$ behavior of the angular distribution of the 127-keV transition into this state and the $\Delta J = 0$ behavior of the 298-keV transition depopulating it to the 8^- metastable state. The corresponding state in ^{118}Sb is probably the one at 473 keV. However, since no angular-distribution information relating to this state is available, we could make no definite assignment.

Finally, we assigned $J = 7$ to the 279-keV state in ^{116}Sb, bases on the $\Delta J = 0$ angular distribution of the 1015- and 54-keV transitions into and out of this state. We found no corresponding state in ^{118}Sb.

IV. DISCUSSION

A. High-Spin Sequences

The high-spin structure of odd-odd Sb nuclei is very closely related to that of the neighboring odd-mass Sb nuclei. This results mainly because of the dominance of the $1h_{11/2}$ unique-parity single-particle orbital, which is readily available for occupancy by the additional odd neutron in these nuclei. Excitation of the $1h_{11/2}$ orbital requires only a few hundred keV of energy and provides at least two additional units of available angular momenta over any other easily-accessible single-neutron state. Consequently, it would be expected that the structure of the yrast levels in both ^{116}Sb and ^{118}Sb should result from a coupling of yrast levels in the neighboring odd-mass Sb nuclei to the high-spin $1h_{11/2}$ neutron state. A qualitative comparison of the odd-odd level schemes to results obtained for the odd-mass Sb nuclei[13-16] supports this suggestion.

There are two obvious candidates for the structures of the $J^{\pi} = 8^-$ metastable states (the "base" states in our high-spin level schemes, located at 225 keV in ^{116}Sb and at 212 keV in ^{118}Sb). The $\pi 2d_{5/2}$ state forms the ground state of the neighboring odd-mass Sb isotopes, with the $\pi 1g_{7/2}$ state a first-excited state decreasing in energy with increasing A until it becomes the ground state at ^{123}Sb. Either of these states could form an 8^- state when coupled with the $\nu 1h_{11/2}$ state; however, measurements of the magnetic moment[8,9] of the J = 8 state in ^{118}Sb favor the $\pi 2d_{5/2} \times \nu 1h_{11/2}$ coupling. [The $\pi 2d_{5/2}$ state appears to be the state involved in the ground-state configurations of these nuclei, as well. In ^{116}Sb it couples with the $3s_{1/2}$ state to produce a 3^+ ground state,[5] and in ^{118}Sb it couples with the

$\nu 2d_{3/2}$ state to produce a 1^+ ground state.[9] Both of these configurations are undoubtedly highly mixed, however.] Actually, the 8^- states may well contain components of both configurations (plus core couplings?), for a straightforward application of the Nordheim coupling rules would not predict the 8^- state to be metastable for either coupling without mixing.

The $\pi 1g_{7/2}$ state (at 724 keV in ^{115}Sb, 527 keV in ^{117}Sb, and 270 keV in ^{119}Sb) and $\pi 1h_{11/2}$ state (at 1300 keV in ^{115}Sb, 1323 keV in ^{117}Sb, and 1366 keV in ^{119}Sb), when coupled to maximum spin with the $\nu 1h_{11/2}$ state, would produce $J^\pi = 9^-$ and 11^+ configurations. These provide plausible candidates for major components of the 9^- and 11^+ states located at 978 and 1624 keV in ^{116}Sb and at 892 and 1695 keV in ^{118}Sb. It should be noted that the 11^+ states, in particular, are far from pure two-particle states. The enhanced transition probability for the E3, $11^+ \rightarrow 8^-$, transition suggests components containing octupole core vibrations. (This same phenomenon occurs for the $11/2^- \rightarrow 5/2^+$ transition in ^{115}Sb and is discussed in terms of the collective model in Ref. 14.)

An additional low-lying high-spin state occurs in the odd-mass Sb nuclei. It has $J^\pi = 9/2^+$, lies in the vicinity of 1300 keV, and can be attributed to the 2^+ single-phonon core excitation coupled to the $\pi 2d_{5/2}$ ground state.[13] Again, coupling this odd-mass Sb state to maximum spin with the $\nu 1h_{11/2}$ state results in a 10^- state. Such states are seen to occur at 1603 keV in ^{116}Sb and at 1523 keV in ^{118}Sb. This same configuration coupled to a lower total spin is the most likely explanation for the $J = 9$ state seen at 1379 keV in ^{118}Sb. We saw no corresponding state in ^{116}Sb.

The higher-lying states have comparable energies to high-spin two-neutron excitations in the Sn core nuclei. Consequently, these states are most likely made up of four-particle states. In addition, these states may

contain deformed components. For example, it has been shown[19] that decoupled, aligned single-particle states coupled to a deformed core make a most efficient system for containing large amounts of angular momentum. Because of the complexity of this situation we can determine little more from the data presently available.

B. Deformed States

An investigation[20] concerning the coexistence of spherical and low-lying deformed states in odd-mass nuclei indicates that such phenomena can occur when the odd nucleon occupies an almost closed-shell configuration. Rotational bands built on low-lying deformed states result from the excitation of quasiparticles out of strongly sloping Nilsson orbitals into the next major shell. Among those nuclei such considerations have been applied to are the odd-mass Sb and Te isotopes.

The odd-mass Sb nuclei have been investigated in considerable detail.[12-15] These experiments clearly indicate a normal rotational-band structure built on low-lying $9/2^+$ states. These bands have been described as resulting from the $9/2^+[404]$ Nilsson orbital, which displays a steep upward slope for prolate deformation, rising above the Fermi level at a deformation of $\beta \approx 0.2$. Consequently, the state is formed by lifting a proton from the filled $1g_{9/2}$ shell-model state, resulting in a strongly-coupled hole state. Because this state is a hole state, the appropriate core nucleus is Te with Z = 52.

In the odd-neutron Te nuclei strongly-coupled rotational bands built on $5/2^+$ and $7/2^+$ states have been observed.[22] These were described as arising from the $5/2^+[402]$ and $7/2^+[404]$ Nilsson orbitals, which again rise sharply for prolate deformation, overcoming the N = 64 subshell gap. As in Sb these again are hole states, which leads to strong coupling. In this case they originate from the $2d_{5/2}$ and $1g_{7/2}$ shell-model states. Which of these bands is more nearly yrast and therefore more favorably excited is determined by the relative position of the Fermi energy with respect to the

Nilsson orbitals. In $^{117}Te_{65}$ and $^{119}Te_{67}$ the $5/2^+$ band is observed, while in $^{121}Te_{69}$ it is the $7/2^+$ band.

The bands in odd-odd Sb nuclei should involve these same Nilsson orbitals. In particular, the $9/2^+[404]$ orbital is the only easily-accessible high-spin candidate available for the proton. Consequently, all of the bands observed in ^{116}Sb and ^{118}Sb can be interpreted here as involving a proton in this orbital. For the neutron, the lower-lying J = 7 bands (located at 1001 keV in ^{116}Sb and at 927 keV in ^{118}Sb) are assigned to the $5/2^+[402]$ orbital. This is reasonable considering that the neutron numbers for these nuclei are the same as for ^{117}Te and ^{119}Te nuclei, where single- particle bands built on this configuration were observed. The bands appear to be relatively normal strongly-coupled bands, which is consistent with the suggested Nilsson configuration. This comes about because both odd-nucleon configurations are hole states and thus for prolate deformation couple to the core. In addition, both orbitals are deformation driving, so the deformation of this two-particle band would be expected to be greater than the deformation in either of the neighboring odd-mass, single- particle bands. This appears to be the case and will be discussed in more detail below.

For the possible J = 7 bands located at 1193 keV in ^{116}Sb and at 927 keV in ^{118}Sb the situation appears to be somewhat more complicated. The energy spacings from J = 9 upward can be reproduced remarkably well by the simple strong-coupling symmetric rotor equation, and it is not bad even from J = 8 upward. However, the resulting value for the rotational constant is $\hbar^2/2 = 16$ keV. This corresponds to a moment of inertia greater than the rigid-rotor value and consequently indicates an alternative description of this band is necessary. A likely explanation for the high apparent moment

of inertia is the decoupling from the core of a high-J single-particle state and the alignment of its angular momentum along the rotation axis. This rotation-alignment coupling scheme is a common phenomenon in odd-mass nuclei[22] and has been extended to describe bands in odd-odd nuclei.[23] For ^{116}Sb and ^{118}Sb the neutron Fermi level, λ_n, lies near the low-Ω components of the $1h_{11/2}$ shell-model state. Such a state is strongly affected by the Coriolis force, which tends to align the particle's angular momentum along the direction of the rotation axis. A very good representation of the Sb bands can be provided by this description. A nearly identical situation occurs in ^{198}Tl and has been described quantitatively by Toki, Yadav, and Faessler.[24] Their technique will be applied here in describing the Sb bands. (A similar analysis has also been performed by Vajda et al.[7])

The angular momentum of the band head is easily determiend by taking the $1g_{9/2}$ proton to be deformation aligned, while the $1h_{11/2}$ neutron is rotationally aligned. Because the angular momenta of the two particles are pointed in perpendicular directions, the resultant angular momentum can be calculated as

$$J \approx (j_p^2 + j_n^2)^{1/2} = [(9/2)^2 + (11/2)^2]^{1/2} = 7.1.$$

This is remarkably close to J = 7 for the bandhead. Experimentally, the two band members below J = 9 display markedly compressed energy spacings as compared to the higher-spin band members. Their inclusion in the band is suggested by the strong intraband transition probabilities linking them to the other members of the bands. This is especially noticeable for the 8 → 7, 37-keV transition in ^{118}Sb. Additionally, the 10 → 8 transition in ^{116}Sb

is an enhanced electric quadrupole crossover transition. Finally, the model used here to describe the bands can reproduce the energy spacing even including the distortion of the low-spin portions of the bands.

There appear to be some simplifying factors in the Sb case which make possible an approximate quantitative understanding of the situation without resorting to the complex calculations that were necessary to describe ^{198}Tl.

First, the deformation for the Sb bands appears to be much larger than for those in Tl. In the Tl region the deformation was determined to be $\beta \approx 0.15$, while for the odd-mass Sb nuclei deformation values as large as $\beta \approx 0.3$ are necessary to describe the data. The result of the larger deformation is that the energy required to change the direction of j_p is much greater. In the odd-mass Tl nuclei, j_p, even though initially deformation aligned, tends to align itself with the rotation axis as the rotational angular momentum increases. The resulting increase in the total particle angular momentum produces a variation in the strength of the residual interaction for normal and non-normal parity states. This appears as a staggering effect in the energy difference between neighboring spin states. The absence of any such staggering effect in the odd-mass Sb bands supports the suggestion that to a good approximation j_p remains aligned with the deformation axis; consequently, the residual interaction has little effect on the band spacing.

Second, the odd-mass Sb bands have been described quite well in terms of a symmetric-rotor model with variable moment of inertia.[25] In the case of ^{198}Tl a triaxial rotor calculation was required.

Finally, if the neutron (proton) Fermi level lies at or below (above) the lowest (highest) Nilsson orbital derived from the $1h_{11/2}$ ($1g_{9/2}$)

shell-model state, then the neutron (proton) can be characterized as a single particle (hole) in an otherwise empty (filled) state. In this case the Pauli Exclusion Principle should be of little consequence, and a classical treatment of the angular momentum vectors should be approximately correct.

Therefore, we fitted the band in ^{116}Sb to a simple, classical, symmetric-rotor model having a variable moment of inertia. In this model j_n is constrained to lie along the direction of the rotation axis, while the direction of j_p is given by θ, the angle it makes with the rotation axis. The rotation angular momentum R can then be determined in terms of θ and J by classical vector addition as given by

$$J^2 = (R + j_n)^2 + J_P^2 + 2j_p(R+j_n)\cos\theta.$$

The energy of the level having total angular momentum J is then found by minimizing with respect to θ the expression,

$$E_J = \frac{\hbar^2}{2\mathcal{J}} R(R+1) + E_{sp}.$$

Here E_{sp}, which depends on θ, represents the single-particle energy required to tilt j_p away from its direction along the deformation axis and toward the rotation axis. Its value is determiend by using the expression for Nilsson energies with the dependence on discrete K values replaced by the corresponding classical angle θ. The expression is normalized such that K = 9/2, which corresponds to $\theta = 90°$, has energy equal to zero. This is equivalent to saying that λ_p is taken to have the value of the highest $1g_{9/2}$ Nilsson level. The result is

$$E_{sp} = (7.6\ \text{MeV})\beta\cos^2\theta.$$

(We treated β, the deformation, as a free parameter.) Because of the softness of the core, a variable moment of inertia is necessary for this calculation. We took it to be

$$\mathcal{J} = \mathcal{J}_0 + AR(R+1),$$

where $\mathcal{J}_0$ is determined from β by means of the normal Grodzins relation[26] and A is left as a free parameter. With these equations the two free parameters, β and A, were varied to produce a good fit to the ^{116}Sb energy spectrum. We performed a similar calculation with $j_n = 0$ in order to describe the neighboring odd-proton ^{115}Sb band. The results of these calculations are shown in Fig. 8. Experimental data for ^{115}Sb are taken from Ref. 14. Considering its simplicity, the model fits the data remarkably well.

Our results indicate that both the odd-odd and odd-mass Sb bands cannot be fit with the same deformation parameter. We obtained β = 0.25 for ^{116}Sb and β = 0.31 for ^{115}Sb, A = 0.00014 for both. This is not unreasonable, however, for this region where the ground states of all nuclei are spherical. (In fact, even in well-deformed nuclear regions the moments of inertia can vary considerably from band to band in the same nucleus, depending on variables such as the degree of Coriolis coupling.) Because the core is soft, deformations can and do occur for specific single-particle states. It is reasonable to expect the value of the deformation to depend on which particular states are occupied. Specifically, the $1g_{9/2}$ proton hole states in the odd-mass Sb nuclei appear to be more deformed than the

$2d_{5/2}$ neutron-hole states in the odd-mass Te nuclei, while the $1h_{11/2}$ neutron-particle states in these same Te nuclei lead to no deformation at all. Consequently, as indicated by the calculation, combining the $\nu 1h_{11/2}$ and $\pi 1g_{9/2}$ states results in a decreased value for β from that obtained for the $\pi 1g_{9/2}$ state alone. Treating the $\nu 2d_{5/2}$ and $\pi 1g_{9/2}$ system in the same manner, however with both j_p and j_n deformation aligned, results in a deformation value ($\beta = 0.36$) which is larger than for the $\pi 1g_{9/2}$ state alone. Thus, it appears that the lower-lying $J = 7$ bands with both particles in strongly coupled, deformation driving orbitals leads to a much more deformed core than the higher-lying $J = 7$ bands, where the neutron is in a decoupled particle state.

The calculation also demonstrates how strongly the $\pi 1g_{9/2}$ state is coupled to the core. The classical tilting of j_p from its deformation-aligned position achieved a maximum of only 9° at $J = 14$. This indicates there is very little Coriolis mixing among the various Nilsson levels derived from the $\pi 1g_{9/2}$ state, which is a bit surprising.

The model can also be used to explain qualitatively the differences that occur for the higher-lying $J = 7$ band in ^{118}Sb. The most noticeable of these differences is the compression of the energy spacing between the first two members of the band. In ^{116}Sb it is 100 keV, while in ^{118}Sb it is only 37 keV. This change can be understood in terms of the increase of the neutron Fermi level, resulting in a change in $\mathcal{J}$ as a function of energy.

As long as λ_n is below the lowest-Ω component of the $\nu 1h_{11/2}$ state it has no effect on the appearance of the band, and the calculation as performed above should describe the situation relatively well. As λ_n increases form the lowest-Ω orbital to the highest, the neutron changes from

a decoupled particle state to a strongly-coupled hole state. In the strong coupling limit the bandhead will have J = 11/2 + 9/2 = 10. Therefore, as the number of neutrons increase, the lower-spin levels in the band should rise in energy relative to the J = 10 state. Also, as the strong-coupling limit is approached, the amount of rotation angular momentum necessary to achieve the higher-spin states (J > 10) is increased because of less particle alignment. This should result in an expansion of the energy spectrum. This effect is also apparent in ^{118}Sb, which displays slightly increased energy spacings for J > 9. Thus, the differences between the higher-lying bands in going from A = 116 to A = 118 can be understood by considering the increase in the neutron Fermi level. (For a detailed treatment of ^{118}Sb, see Ref. 7.)

To conclude, the rotational bands in ^{116}Sb and ^{118}Sb can be accounted for by a simple symmetric-rotor model having a variable moment of inertia. The accuracy with which this model fits the higher-lying J = 7 band in ^{116}Sb indicates that it provides a good understanding of what is actually happening in this system. It should be emphasized, however, that energy levels alone do not provide a very sensitive test to any model. It is possible that an equally good alternative description of these bands might exist. In particular, the introduction of a triaxial degree of freedom might allow the various bands to be described with the same deformation parameter. This, however, appears unlikely, if only from the magnitude of the β discrepancies involved. More likely the case is that the core in this region, as indicated by the symmetric-rotor calculation, is extremely soft, and the deformation has a strong dependence on the particular intrinsic states involved.

Acknowledgments

We thank Prof. H. Toki for valuable suggestions and helping us with the rotational-band calculations. We also thank Dr. R. Aryaeinejad and Ms. W.-T. Chou for helpful suggestions and for a critical reading of the manuscript. This work was supported by the U.S. National Science Foundation under Grant #PHY-83-12245.

References

[1]R. Kamermans, H. W. Jongsma, T. J. Ketel, R. van der Way, and H. Verheul, Nucl. Phys. A266, 346 (1976).

H.-E. Mahnke, E. Dafni, M. H. Rafailovich, G. D. Sprouse, and E. Vapirev, Phys. Rev. C 26, 493 (1982).

[3]P. van Nes, W. H. A. Hesselink, W. H. Dickhoff, J. J. van Ruyven, M. J. A. de Voigt, and H. Verheul, Nucl. Phys. A379, 35 (1982).

[4]R. Duffait, J. van Maldeghem, A. Charvet, J. Sau, K. Heyde, A. Emsallem, M. Meyer, R. Beraud, J. Treherne, and J. Genevey, Z. Phys. A 307, 259 (1982).

[5]C. B. Morgan, Ph. D. Thesis, Michigan State University, 1975 (unpublished).

[6]C. B. Morgan, W. H. Bentley, R. A. Warner, W. H. Kelly, and Wm. C. McHarris, Phys. Rev. C 23, 1228 (1981).

S. Vajda, W. F. Piel, M. A. Quader, W. A. Watson, F. C. Yang, and D. B. Fossan, Phys. Rec. C 27, 2995 (1983).

S. Dima, M. Duma, M. Ionescu-Bujor, A. Iordăchescu, G. Pascovici, and C. Stan-Sion, Z. Phys. A 320, 613 (1985).

[9]Wm. B. Chaffee, Wm. C. McHarris, and W. H. Kelly, Phys. Rec. C (in press).

[10]R. A. Emigh, C. A. Fields, M. L. Gartner, L. E. Samuelson, and P. A. Smith, Z. Phys. A 308, 165 (1982).

[11]R. A. Emigh, C. A. Fields, M. L. Gartner, L. E. Samuelson, and P. A. Smith, Z. Phys. A 308, 173 (1982).

[12]V. L. Alexeev, B. A. Emelianov, A. I. Egorov, L. P. Kabina, D. M. Kaminker, Yu. L. Khazov, I. A. Kondurov, E. K. Leushkin, Yu. E. Loginov, V. V. Martynov, V. L. Rumiantsev, S. L. Sakharov, P. A. Sushkov, H. G.

Börner, W. F. Davidson, J. A. Pinston, and K. Schreckenbach, Nucl. Phys. A297, 373 (1978).

[13]R. E. Shroy, A. K. Gaigalas, G. Schatz, and D. B. Fossan, Phys. Rev. C 19, 1324 (1979).

[14]J. Bron, W. H. A. Hesselink, H. Bedet, H. Verheul, and G. vanden Berghe, Nucl. Phys. A297, 365 (1977).

[15]W. D. Fromm, H. F. Brinckmann, F. Dönau, C. Heiser, F. R. May, V. V. Pashkevich, and H. Rotter, Nucl. Phys. A243, 9 (1975).

[16]W. F. Piel, C. Chowdhury, U. Garg, M. A. Quader, P. M. Swertka, S. Vajda, and D. B. Fossan, Phys. Rev. C 31, 456 (1985).

[17]G. H. Carlson, W. L. Talbert, and S. Raman, Nucl. Data Sheets 17, 17 (1976).

[18]C. Ekström, W. Horgervorst, S. Ingelman, and G. Wannberg, Nucl. Phys. A226, 219 (1974).

[19]M. F. Slaughter, R. A. Warner, T. L. Khoo, W. H. Kelly, and Wm. C. McHarris, Phys. Rev. C 29, 114 (1984).

[20]K. Heyde, M. Waroquier, H. Vincx, and P. van Isacker, Phys. Lett. 64B, 136 (1976).

[21]U. Hagemann, H.-J. Keller, Ch. Protochristow, and F. Stary, Z. Phys. A 290, 399 (1979).

[22]F. S. Stephens, Rev. Mod. Phys. 47, 43 (1975).

[23]H. Toki and A. Faessler, Nucl. Phys. A253, 23 (1975).

[24]H. Toki, H. L. Yadav, and A. Faessler, Phys. Lett. 71B, 1 (1977).

[25]P. C. Simms, F. A. Rickey, and R. K. Popli, Nucl. Phys. A347, 205 (1980).

[26]L. Grodzins, Phys. Lett. 2, 88 (1962).

Table I. ^{116}Sb γ-Ray Data

E_γ[a] (keV)	I_γ[b]	A_2/A_0	A_4/A_0	$J_i \rightarrow J_f$	δ
21.6[c]	1.7			11 → 10	
53.5	27.0	-0.15±0.05	0.09±0.08	7 → 8	
99.8[d]	41.5	-0.18±0.10		8 → 7	
121.8	2.5	0.11±0.04	0.28±0.07		
127.4	0.8	-0.410.12	0.00±0.25	7 → 8	
142.2[c]	0.7				
192.6	11.8	0.31+0.02	-0.06±0.04	7 → 7	
215.1	50.6	-0.07±0.02	-0.02±0.06	9 → 8	0.18<δ< 0.21
226.2	8.1	-0.91±0.02	0.08±0.04	15 → 14	-1.25<δ<-0.68
240.6	23.0	0.63±0.03	0.22±0.05	14 → 13	0.86<δ< 1.37
298.4	18.3	0.04±0.03	-0.01±0.06	8 → 8	
317.2	41.1	-0.03±0.03	0.02+0.04	10 → 9	0.10<δ< 0.14
341.1[e]	1.9	-0.30±0.09		(11) → 10	
349.5	16.8	0.14±0.03	0.00±0.06	7 → 7	-0.55<δ<-0.41
352.0[c]	27.2			(11) → 10	
382.3	14.7	-0.07±0.03	0.01±0.04	(12) → (11)	0.07<δ< 0.11
389.1[c]	1.0				
404.9	6.8	0.19±0.06	0.00±0.11	(9) → (8)	0.24<δ< 0.33
410.0[c]	10.0			(13) → (12)	
410.9[c]	21.4			(8) → (7)	
423.7	5.0	0.08±0.04	0.02±0.07	(10) → (9)	0.17<δ< 0.23
426.2	47.3	-0.11±0.02	-0.02±0.04	7 → 8	-0.14<δ<-0.01

435.3[c]	2.5			(11) → (10)	
443.8[e]	7.1	0.03±0.07		(14) → (13)	0.11<δ< 0.21
467.1	27.6	0.29±0.03	-0.06±0.05	15 → 13	
480.0	7.5	-0.33±0.04	-0.08±0.05	(8) → 7	
507.0[c]	14.0				
532.4	3.9	0.35±0.04	-0.03±0.06	10 → 8	
542.2[d]	8.1	0.50±0.30		7 → 7	
597.5[e]	14.3	0.09±0.06			
625.0	3.5	-0.51±0.05	-0.10±0.07	10 → 9	
641.9	5.0	-0.07±0.03	0.01±0.06	8 → 7	0.07<δ< 0.13
646.7	14.3	0.41±0.02	-0.02±0.04	11 → 9	0.07<δ< 0.13
669.2[c]	6.0			(11) → 9	
669.4[c]				(11) → (11)	
669.8[c]	7.0			7 → 8	
684.3[e]	4.6	-0.47±0.08			
734.7[c]	6.0			(12) → 10	
752.6	8.0				
752.8	58.3	-0.58±0.03	-0.03±0.06	9 → 8	-0.28<δ>-0.22
775.7	25.1	-0.14±0.02	-0.06+0.04	7 → 8	-0.03<δ< 0.01
792.3	4.6	0.44±0.09	-0.13±0.16	13 → 11	
828.7[e]	3.1	0.36±0.10		(10) → (8)	
846.6	12.9	0.03±0.05	-0.04±0.08		
854.0[c]	3.6			(14) → (12)	
859.2	5.6	0.31±0.07	-0.13±0.12	(11) → (9)	
906.1[c]	2.9			(8) → (8)	
968.4	38.0	-0.26±0.02	-0.01±0.03	7 → 8	
1014.5	24.9	-0.09±0.03	-0.01±0.04	8 → 7	

1021.4	13.9	-0.18±0.03		(11) → 10	
1110.2[e]	3.3	-0.31±0.12			
1122.0	18.9	-0.75±0.02	0.07±0.04	(13) → (12)	
1184.0	70.5	0.31±0.02	-0.09±0.03	13 → 11	
1283.2	6.0	-0.47±0.07	-0.06±0.11	9 → 8	$-0.21<\delta<-0.10$
1377.6	33.0	0.27±0.02	-0.09±0.03	10 → 8	
1399.1	100.0	0.53±0.02	0.05±0.04	11 → 8	
1504.3[c]				(13) → (11)	

[a]Energy uncertainties are 0.2 keV for most transitions, rising to 0.5 keV for weak transitions and components of multiplets.

[b]Intensity uncertinties are approximately 15% for most transitions, rising to 30% for weak transitions and components of multiplets.

[c]These are transitions that are too weak to fit or are components of unresolvable multiplets.

[d]Coefficients for these transitions were obtained by subtracting appropriate amounts of ^{116}Sb peaks, as calculated from known intensity ratios.

[e]Weak transitions for which A_0 was set to 0 during the fitting procedure.

Table II. ^{118}Sb γ-Ray Data

E_γ[a] (keV)	I_γ[b]	A_2/A_0	A_4/A_0	$J_i \rightarrow J_f$
37.1[c]				(8) → 7
57.5	13.7			
108.8	8.7	-0.25±0.09	-0.05±0.14	
152.1[d]	5.4	0.62±0.20		(10) → 10
161.4	57.4	-0.29±0.07	0.01±0.10	11 → 10
202.7[e]	44.0			11 → 10
222.5	17.7	0.37±0.03	-0.05±0.04	7 → 7
253.2[e]	31.7			
261.0	40.3	0.11±0.02	0.01±0.03	
297.4[d]	2.4	-0.26±0.12		7 → (8)
305.9[d]	10.2			(10) → 9
318.3	100.0	-0.09±0.01	-0.06±0.04	7 → 8
321.6	9.5	-0.18±0.04	-0.05±0.05	(8) → 7
326.1	44.3	-0.02±0.05	-0.03±0.07	10 → 9
361.9	24.8	-0.03±0.03	0.00±0.04	11 → 10
371.0	18.5	0.30±0.03	-0.01±0.04	8 → 7
376.0	15.3	0.20±0.06	-0.12±0.09	9 → 8
377.8	8.8			
387.4[e]	19.6			(12) → 11
392.6[d]	5.2	0.22±0.17		10 → 9
396.7	38.3	0.11±0.01	-0.06±0.01	7 → 7
415.1[e]	13.1			13 → 12
418.6[e]	3.1			(11) → 10

480.7[e]	19.1			
489.9[e]	6.2			
619.0[e]	6.3			7 → 7
640.8	2.5			10 → 9
671.2[e]	40.5			
676.5[e]	6.9			
680.2	46.9	-0.60±0.02	0.01±0.02	9 8
714.8	15.4	-0.09±0.02	-0.04±0.04	7 → 8
746.9[e]				9 → 7
768.5[e]	2.0			10 → 8
793.1	11.8			(10) → 9
937.3	44.8	-0.24±0.05	-0.02±0.08	7 → 8
1167.3	29.4	-0.99±0.07	0.12±0.10	9 → 8
1177.1[d]	28.3	-0.67±0.19		9 → 8
1321.1	75.4	0.17±0.04	-0.21±0.07	10 → 8

[a]Energy uncertainties are 0.2 keV for most transitions, rising to 0.5 keV for weak transitions and components of multiplets

[b]Intensity uncertainties are approximately 15% for most transitions rising to 30% for weak transitions and components of multiplets.

[c]This transition was not observed directly. It energy was determined from level-energy differences.

[d]Coefficients for these transitions were obtained by subtracting appropriate amounts of interfering ^{116}Sb peaks, as calculated from known intensity ratios.

[e]Transitions too weak to fit or components of unresolvable multiplets.

Table III. ^{116}Sb Coincidence Data

Gate Energy (keV)	Coincident γ-Rays (keV)
100[a]	136,[a,b] 193, 215, (298), 317, 341, 352, 382, 389, 407,[a,b] 410, 426, (444), 542,[a] 776, 847, 968, 973,[a,b] 1021, 1294[a,b]
193	100, (142), 215, 317, 350, 352, 382, 410, 426, (444), 562,[e] 776
215[c]	100, 193, 207,[b,c] 298, 317, 341, 352, 382, 389, 410, 426, 442,[b,c] 444, 542, 669, (735), 776, (792), 968, (1021)
226	241, 507, 753, 1184
241	226, (507), 598, 1184, 1399
298	(127), (215), 350, 670
317	100, (133),[b] 193, 215, 294,[b] 320,[b] 341, 352, 382, 407,[b] 410, 426, 542, (735), (776), 968, (1021)
341	100, 215, 317, 389
350[d]	100, 193, 197,[b,c] 202,[b,c] 215, 317, (352), (382), 411, 426, (527),[b,c] (1000)
352[e]	100, 103,[b,e] 157,[b,e] 193, 215, 317, (341), (350), 382, 410, 426, 444, (532), (542), 776, (792), 968, (1283), 1504

382	100, 193, 215, 298, 317, 352, 405,[b] 410, 426, 444, 669, (839),[b] (854), 968, (1122)
405[a]	92,[b] 100,[a,b] 136,[a,b] 319,[b] 381,[b] 392,[b] 411, 424, 426, 437 ,[a,b] (467),[b] 776, (859), 973,[a,b], 1072,[a,b] 1294[a,b]
411[e]	92,[b,e] 100, 215, 224,[b,e] 317, 338,[b,e], 352, 382, 392,[b] 405,[e] (411),[b] 424, 426, 435, 776, (829), (859), 968
424	(392),[b] 405, 411, 435, 529,[b] (776)
426	100, 193, 215, 317, 341, 350, 352, 382, (405), 410, 411, (424), 480, 542, (642), 684
444	100, 215, 317, (352), (382), 410, (792)
467	507, 598, (753), 1184, 1399
480	426
507	(226), (753)
532	100, (215),[b] (240),[b] (255),[b] 352, 382, (410), (933)[b]
542[a]	100,[a] 136,[a,b] 215, (294),[b] 317, (382), 426, (582),[b] 973,[a,b] 1072,[a,b] 1294[a,b]
598	(241), (407),[b] (467), (1184), (1399)
647	241, 753, 1184
670	100, 215, (298), (317), (352), (382)
753	(241), (317), (624), 647, 1021
776	(100), 215, 317, (352), (405), 411
968	100, 215, 317, 352, 382, 410

1015	215, (317), (352)
1184	(226), 241, 331,[b] 467, 507, (598), (753), (840),[b] (886),[b] 1399
1399	241, (336),[b] (392),[b] 467, (495),[b] 598, 1184

[a] A transition of this energy is known to occur in ^{116}Sn.

[b] These transitions have not been placed in the level scheme.

[c] A transition of this energy is known to occur in ^{115}Sb.

[d] A transition of this energy is known to occur in ^{117}Sb.

[e] A transition of this energy is known to occur in the low-spin level scheme of ^{116}Sb.

Table IV. ^{118}Sb Coincidence Data

Gate Energy (keV)	Coincident γ-Rays (keV)
109	253, 318
152	1321
161	368,[a] 378, 481, 490, 600,[a] (641), 671, 1321
203[b,c]	96,[a,b] 153,[a,c] 223, (237),[a,c] 261, 297, 318, 326, 362, 387, 397, 415, 465,[a] 507,[a,c] (619), (677), (715), 937
123	203, 318, 326, 362, 397, 715, (749)[a]
253[d]	109, 318, 1051,[a,d] (1092),[a,d] 1230[a,d]
261[e]	203, 231,[a,e] 326, 345,[a,e] (362), 415, 490,[a] 677, 690[a,e]
297	(203)
306	1167
318	109, 203, 223, 253, 322, 326, 362, 371, 376, 387, 393, 397, (404),[a] 580,[a] 619, (836),[a] (1014)[a]
322	(203), 297, 318
326	203, 223, 297, 318, 362, 387, 397, (415), 937, 1177
362[f]	135,[a,f] 203, 223, 270,[a,f] 318, 326, 335,[a,f] 370,[a,f] 382,[a,f] 387, 397, (415), 700,[a,f] (937)

371[f]	135,[a,f] 270,[a,f] 318, 335,[a,f] 362,[a,f] 376, 382,[a,f] 393, 397, (419), (444),[a] (660),[a] 700[a,f] 715, 769
376[c,g]	115[a,c] 254,[a] 261, 318, 337,[a,g] 366,[a,g] 371, (393), 297, (419), (907),[a] 1160[c,g]
378	161, 671, 1321
387	203, (223), 253,[a] 270,[a] 326, 362, 397, 415
393	318, 371, 376, 397, (404),[a] 419, (715), (907)[a]
397	203, 223, (254),[a] 261, 318, 326, (362), 371, 376, 393, 419, 747
415[c,h]	203, 209,[a,c] 273,[a,c] 304,[a,c] 326, 362, (387), 795,[a] 819,[a,h] 1294[a,h]
418	161, (190),[a] 671, (1321)
490	(161), 190,[a] (481), (671), 842,[a] (1321)
619	318
671	(152), 161, (242),[a] 378, (391),[a] 481, (490), 1321
677	261
680	793, 941[a]
793	680
937[i]	183,[a,i] 203, 326

1167	306
1177	326, 362
1321	153, 161, (378), (481), 671

[a]These transitions have not been placed in the level scheme.

[b]A transition of this energy is known to occur in ^{116}In.

[c]A transition of this energy is known to occur in the low-spin level scheme of ^{118}Sb.

[d]A transition of this energy is known to occur in ^{118}Sn.

[e]A transition of this energy is known to occur in ^{115}In.

[f]A transition of this energy is known to occur in ^{119}Sb.

[g]A transition of this energy is known to occur in ^{117}Sb.

[h]A transition of this energy is known to occur in ^{116}Sn.

[i]A transition of this energy is known to occur in ^{18}F.

Table V. Half-Lives of Metastable States

E_x (keV)	E_γ (keV)	Half-Life (nsec)
^{116}Sb:		
1001	776	12.8±0.2
	426	12.3±0.2
		12.6±0.2 adopted
1072	847	2.4±0.2
1624	1399	4.1±0.1
	1377	4.0±0.2
	753	4.3±0.1
	647	4.0±0.2
		4.1±0.1 adopted
1193	193	1.0±0.5
3049	1184	1.4±0.5
	240	1.2±0.5
		1.3±0.4 adopted

3599	1021	7.7±1.2
	317	6.6±0.5
	215	7.2±0.2
		7.1±0.2 adopted

---

^{118}Sb:

927	318	23.5±1.3
	397	20.0±0.6
		21.7±1.4 adopted

==========

Figure Captions:

Fig. 1. γ-ray spectrum from the reaction, $^{115}In(\alpha,3n\gamma)^{116}Sb$, taken at 130° with respect to the beam direction. Peaks labelled (5) come from ^{115}Sb; (7), from ^{117}Sb.

Fig. 2. Angular distributions for selected ^{116}Sb γ-transitions. The fits are normalized to 1.0 at 90°.

Fig. 3. γ-ray spectrum from the reaction, $^{120}Sn(p,3n\gamma)^{118}Sb$, taken at 125° with respect to the beam direction.

Fig. 4. Excitation functions for γ-transitions in ^{118}Sb.

Fig. 5. γ-ray spectrum from the reaction, $^{114}Cd(^{7}Li,3n\gamma)^{118}Sb$, taken at 125° with respect to the beam direction.

Fig. 6. High-spin level scheme for ^{116}Sb.

Fig. 7. High-spin level scheme for ^{118}Sb.

Fig. 8. Comparisons of experimental levels in ^{116}Sb with those calculated using a symmetric-rotor model having a variable moment of inertia. j_n was constrained to lie in the direction of the core rotation, while θ (see text) gives the direction of j_p with respect to the

core-rotation axis. A similar calculation was made for the levels in ^{115}Sb for a control comparison.

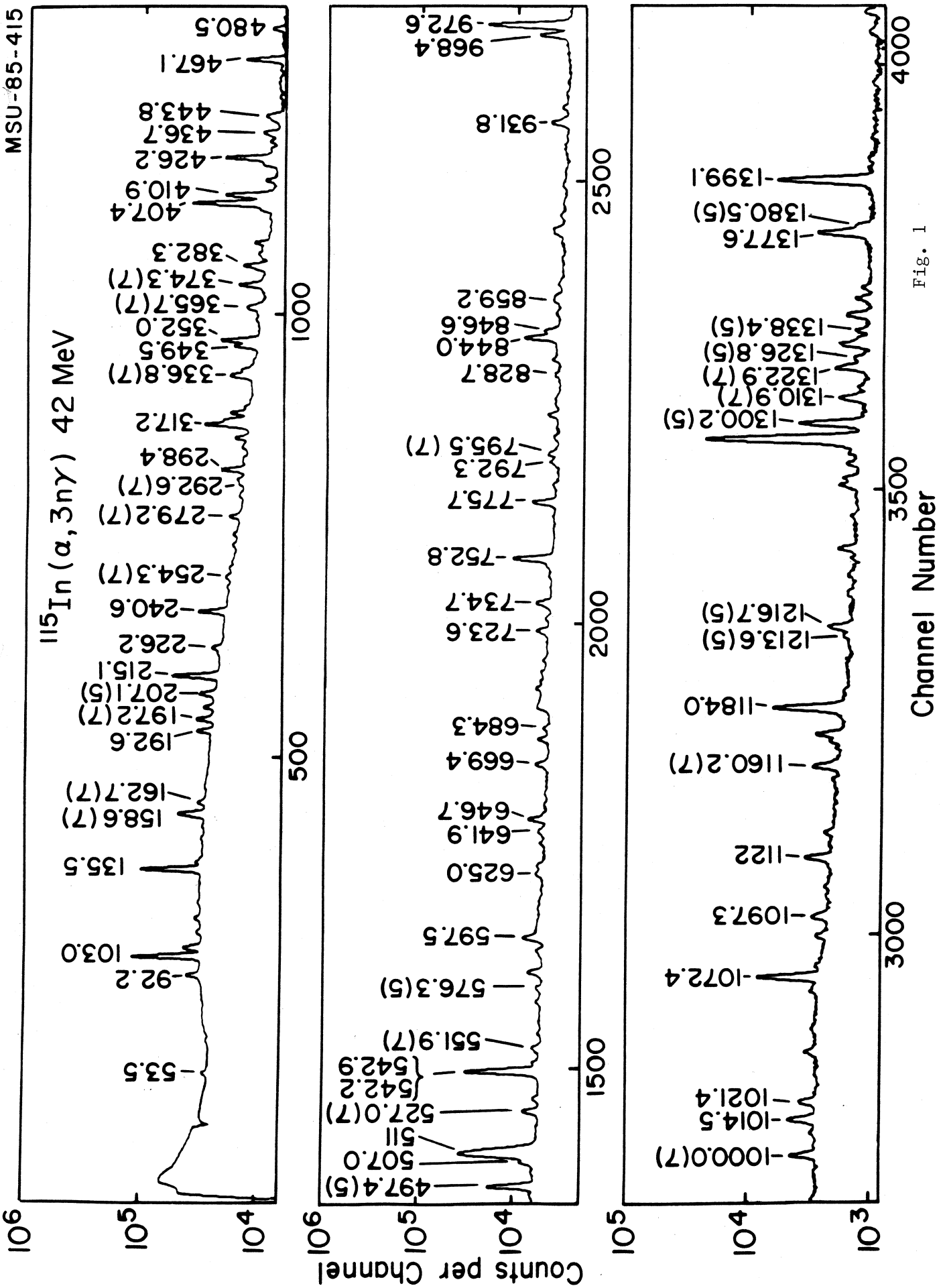
MSU-85-415
^{115}In(α,3nγ) 42 MeV
Counts per Channel
Channel Number
53.5
92.2
103.0
135.5
158.6(7)
162.7(7)
192.6
197.2(7)
207.1(5)
215.1
226.2
240.6
254.3(7)
279.2(7)
292.6(7)
298.4
317.2
336.8(7)
349.5
352.0
365.7(7)
374.3(7)
382.3
407.4
410.9
426.2
436.7
443.8
467.1
480.5
497.4(5)
507.0
511
527.0(7)
542.2
542.9
551.9(7)
576.3(5)
597.5
625.0
641.9
646.7
669.4
684.3
723.6
734.7
752.8
775.7
792.3
795.5 (7)
828.7
844.0
846.6
859.2
931.8
968.4
972.6
1000.0(7)
1014.5
1021.4
1072.4
1097.3
1122
1160.2(7)
1184.0
1213.6(5)
1216.7(5)
1300.2(5)
1310.9(7)
1322.9 (7)
1326.8(5)
1338.4(5)
1377.6
1380.5(5)
1399.1

Fig. 1

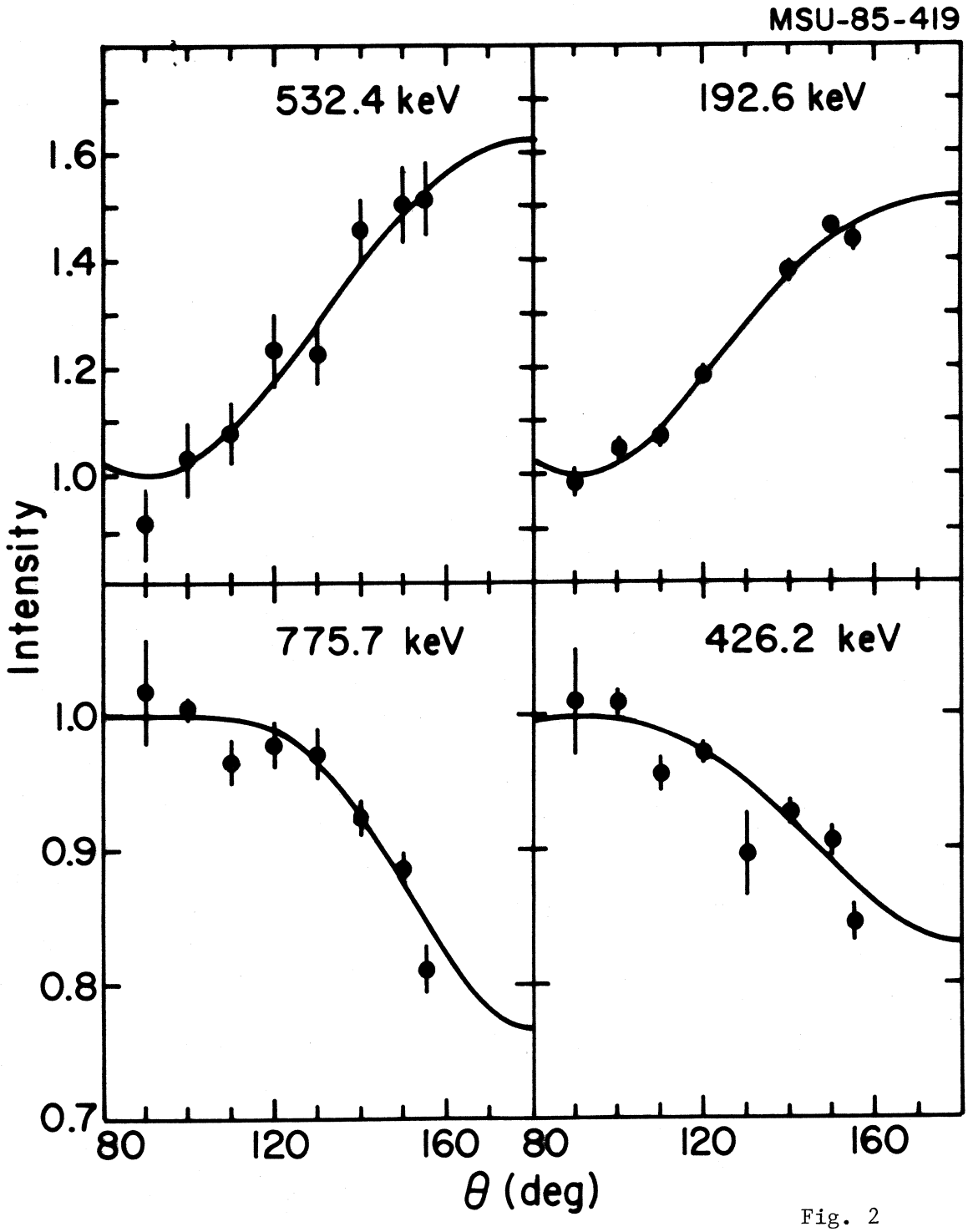
MSU-85-419
532.4 keV
192.6 keV
775.7 keV
426.2 keV
Intensity
1.6
1.4
1.2
1.0
0.9
0.8
0.7
80
120
160
θ (deg)

Fig. 2

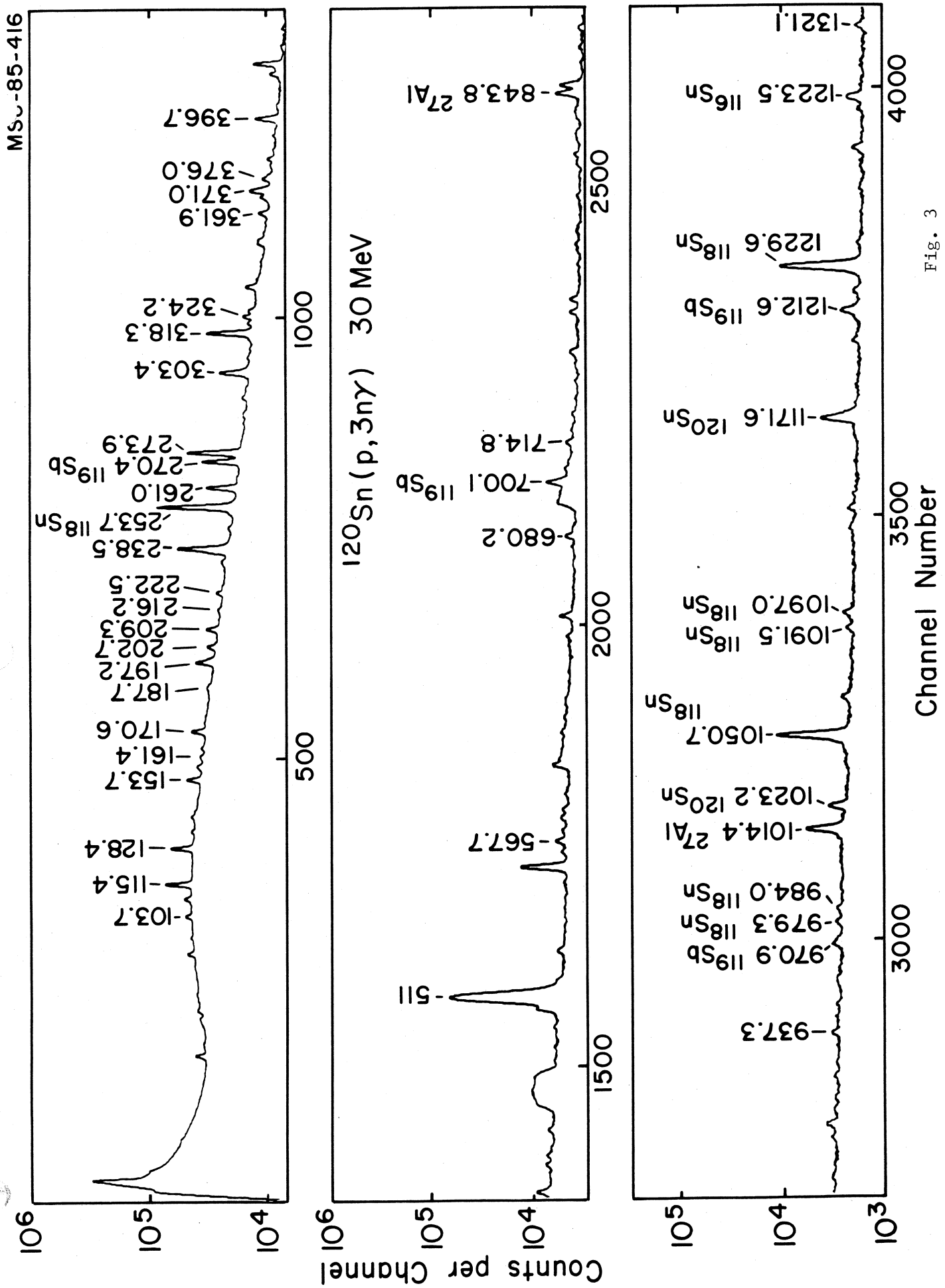
MSU-85-416
103.7
115.4
128.4
153.7
161.4
170.6
187.7
197.2
202.7
209.3
216.2
222.5
238.5
253.7 118Sn
261.0
270.4 119Sb
273.9
303.4
318.3
324.2
361.9
371.0
376.0
396.7
120Sn (p,3nγ) 30 MeV
511
567.7
680.2
700.1 119Sb
714.8
843.8 27Al
937.3
970.9 119Sb
979.3 118Sn
984.0 118Sn
1014.4 27Al
1023.2 120Sn
1050.7 118Sn
1091.5 118Sn
1097.0 118Sn
1171.6 120Sn
1212.6 119Sb
1229.6 118Sn
1223.5 116Sn
1321.1
Counts per Channel
Channel Number

Fig. 3

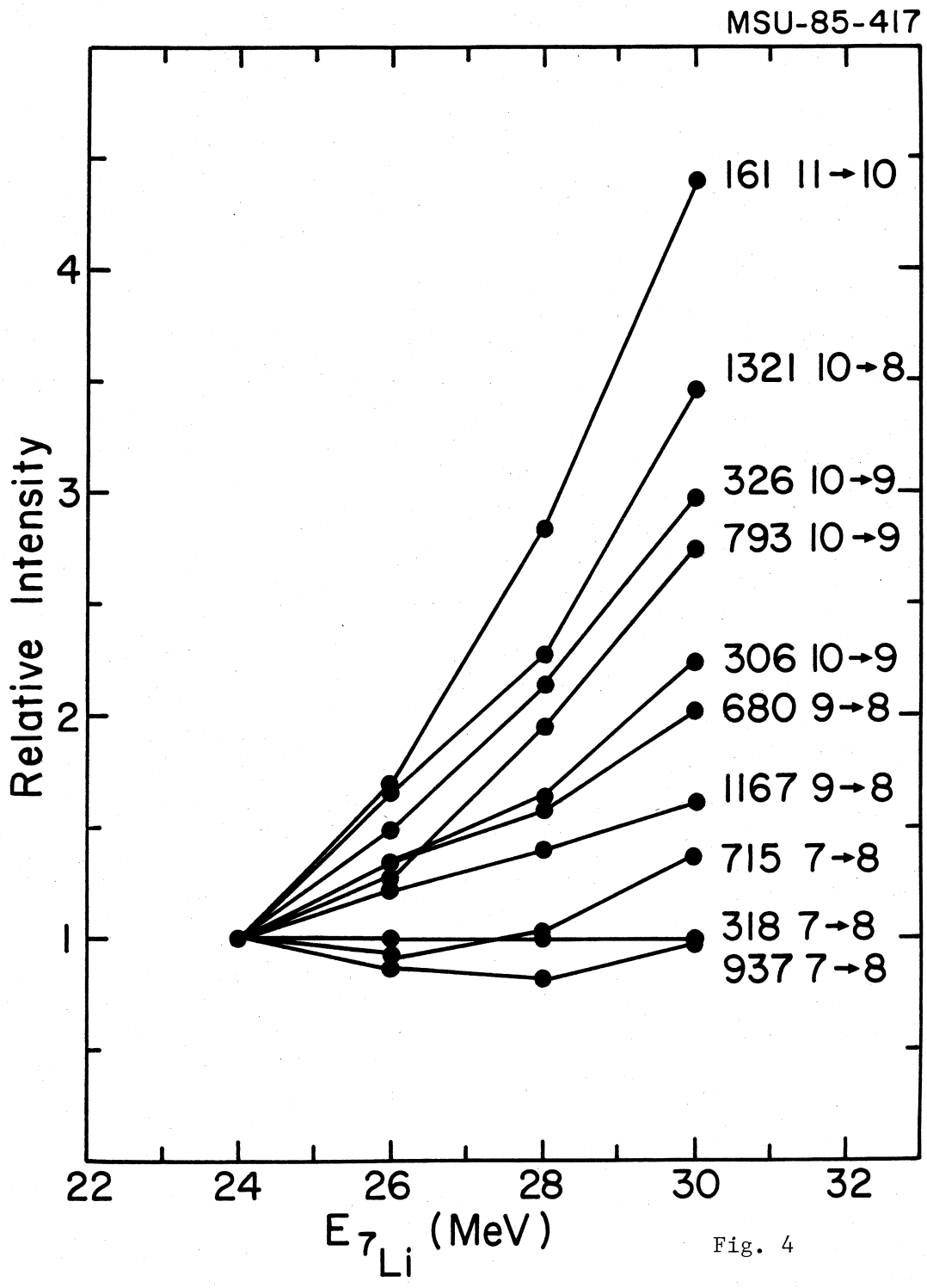
MSU-85-417
161 11→10
1321 10→8
326 10→9
793 10→9
306 10→9
680 9→8
1167 9→8
715 7→8
318 7→8
937 7→8
Relative Intensity
1
2
3
4
22
24
26
28
30
32
E 7Li (MeV)

Fig. 4

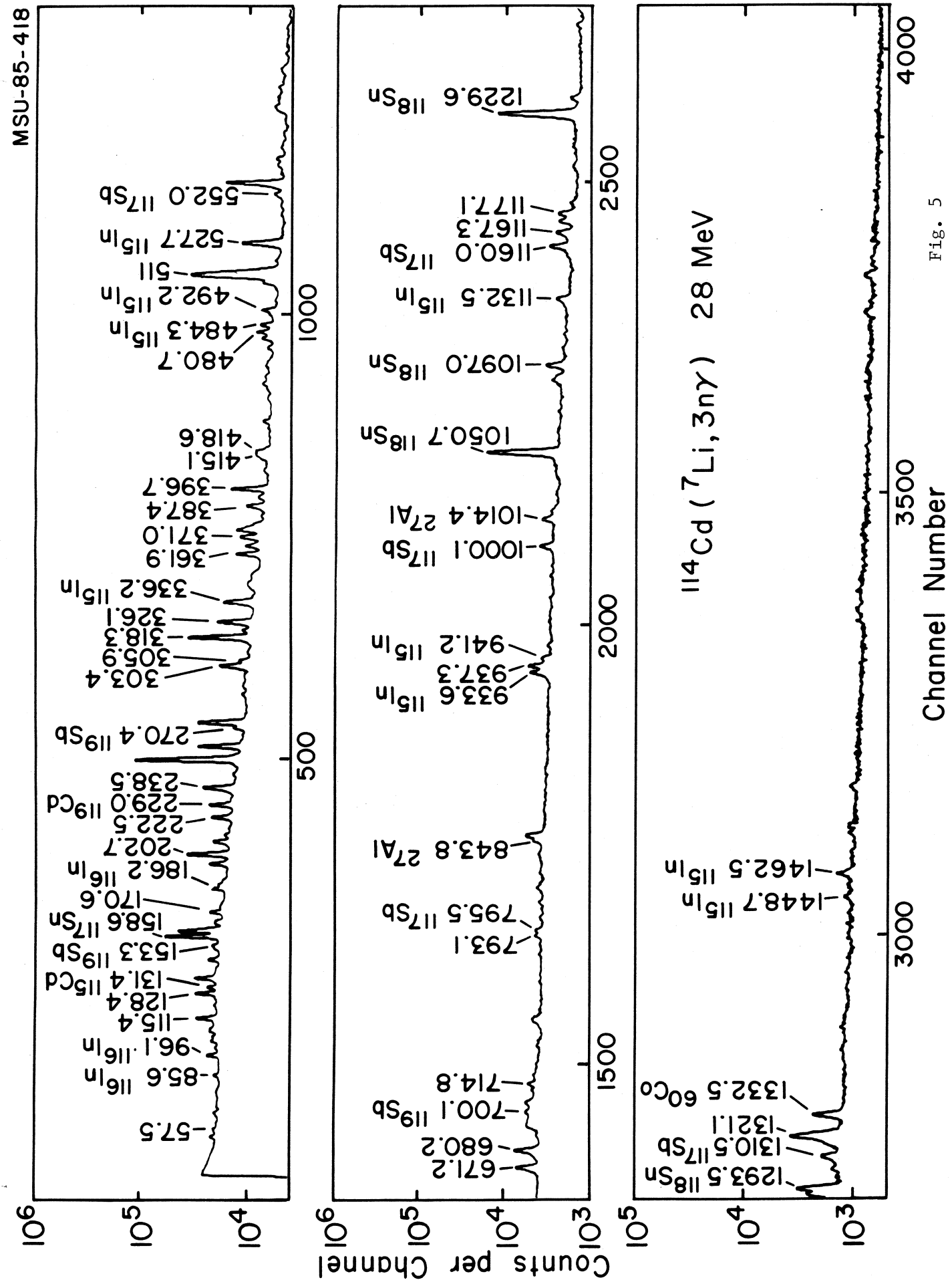
MSU-85-418
^{114}Cd (^{7}Li, 3nγ) 28 MeV
Counts per Channel
Channel Number
1293.5 ^{118}Sn
1310.5 ^{117}Sb
1321.1
1332.5 ^{60}Co
1448.7 ^{115}In
1462.5 ^{115}In
671.2
680.2
700.1 ^{119}Sb
714.8
793.1
795.5 ^{117}Sb
843.8 ^{27}Al
933.6 ^{115}In
937.3
941.2 ^{115}In
1000.1 ^{117}Sb
1014.4 ^{27}Al
1050.7 ^{118}Sn
1097.0 ^{118}Sn
1132.5 ^{115}In
1160.0 ^{117}Sb
1167.3
1177.1
1229.6 ^{118}Sn
57.5
85.6 ^{116}In
96.1 ^{116}In
115.4
128.4
131.4 ^{115}Cd
153.3 ^{119}Sb
158.6 ^{117}Sn
170.6
186.2 ^{116}In
202.7
222.5
229.0 ^{119}Cd
238.5
270.4 ^{119}Sb
303.4
305.9
318.3
326.1
336.2 ^{115}In
361.9
371.0
387.4
396.7
415.1
418.6
480.7
484.3 ^{115}In
492.2 ^{115}In
511
527.7 ^{115}In
552.0 ^{117}Sb

Fig. 5

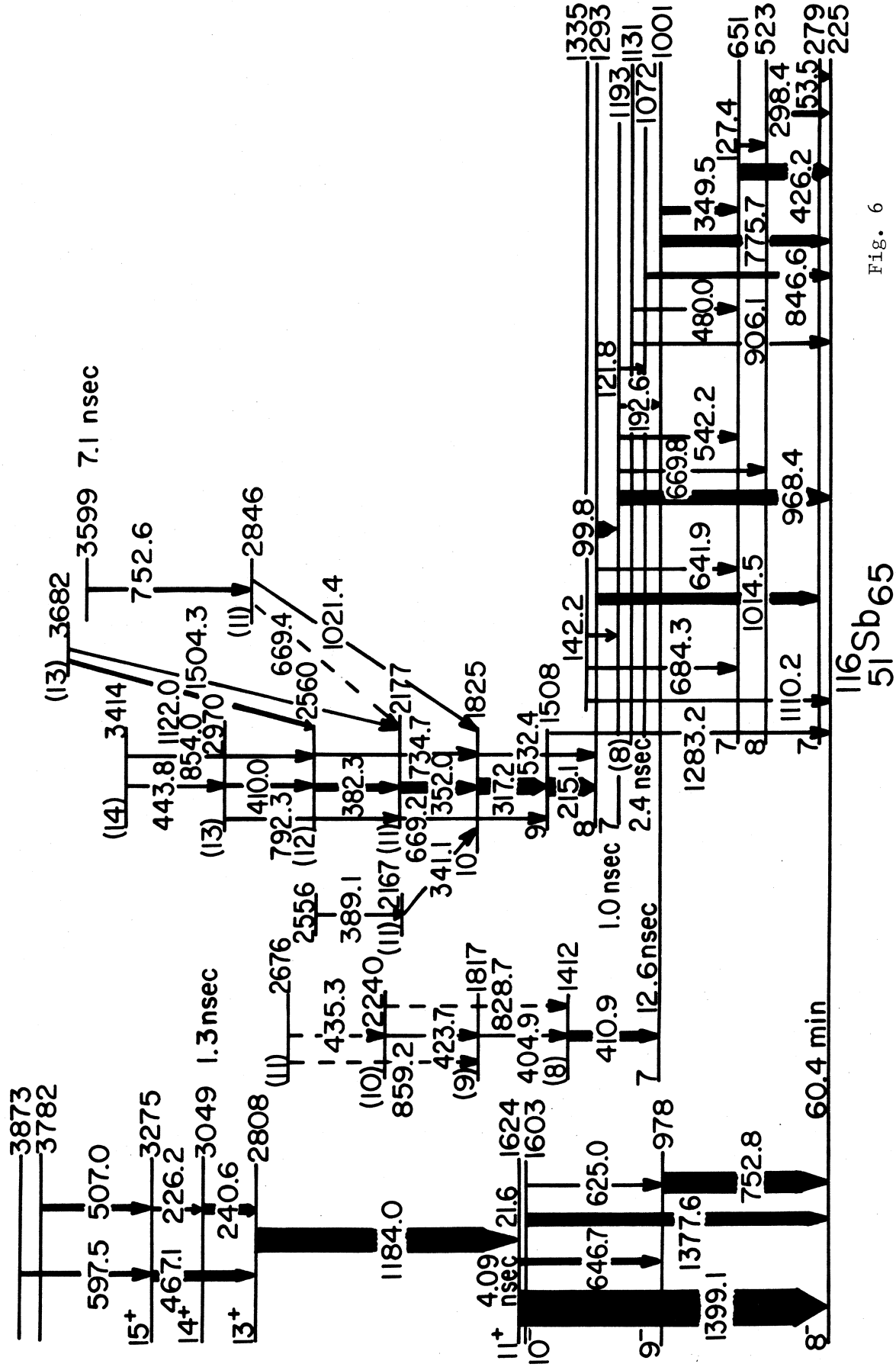
MSU-85-429
$^{116}_{51}Sb_{65}$
60.4 min
12.6 nsec
2.4 nsec
1.0 nsec
1.3 nsec
4.09 nsec
7.1 nsec
15+
14+
13+
11+
10−
9−
8−
3873
3782
3599
3682
3414
3275
3049
2846
2808
2676
2556
2240
1817
1624
1603
1508
1412
978
3873
3782
507.0
597.5
467.1
226.2
240.6
1184.0
21.6
752.6
1504.3
1122.0
854.0
443.8
2970
4100
792.3
669.4
2560
1021.4
2177
1825
734.7
382.3
352.0
669.2
317.2
532.4
215.1
389.1
2167
341.1
435.3
859.2
423.7
828.7
404.91
410.9
625.0
646.7
1377.6
1399.1
752.8
99.8
142.2
121.8
192.6
669.8
542.2
641.9
684.3
1014.5
1283.2
1110.2
968.4
480.0
906.1
846.6
349.5
775.7
426.2
127.4
298.4
153.5
1335
1293
1193
1131
1072
1001
651
523
279
225

Fig. 6

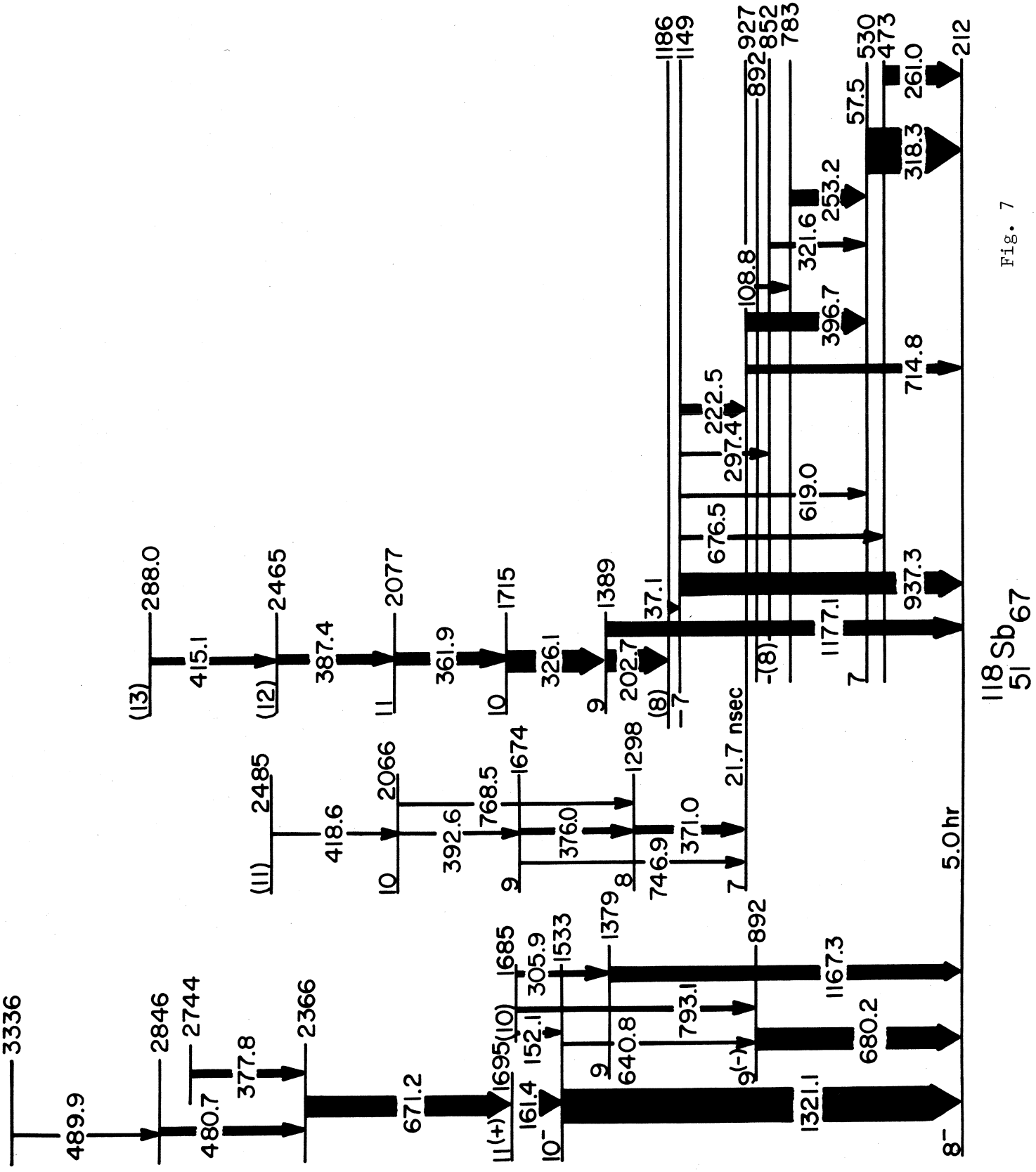
MSU-85-428
$^{118}_{51}Sb_{67}$
5.0hr
21.7 nsec
8⁻
10⁻
11(+)
(13)
(12)
(11)
(10)
(8)
3336
2846
2744
2366
2485
2465
2077
2066
1715
1674
1389
1298
1695
1685
1533
1379
892
489.9
480.7
377.8
671.2
418.6
415.1
387.4
392.6
361.9
768.5
326.1
376.0
202.7
746.9
371.0
288.0
161.4
152.1
305.9
640.8
793.1
1321.1
1167.3
680.2
1186
1149
927
892
852
783
530
473
261.0
212
57.5
318.3
253.2
321.6
108.8
396.7
714.8
222.5
297.4
619.0
676.5
37.1
937.3
1177.1

Fig. 7

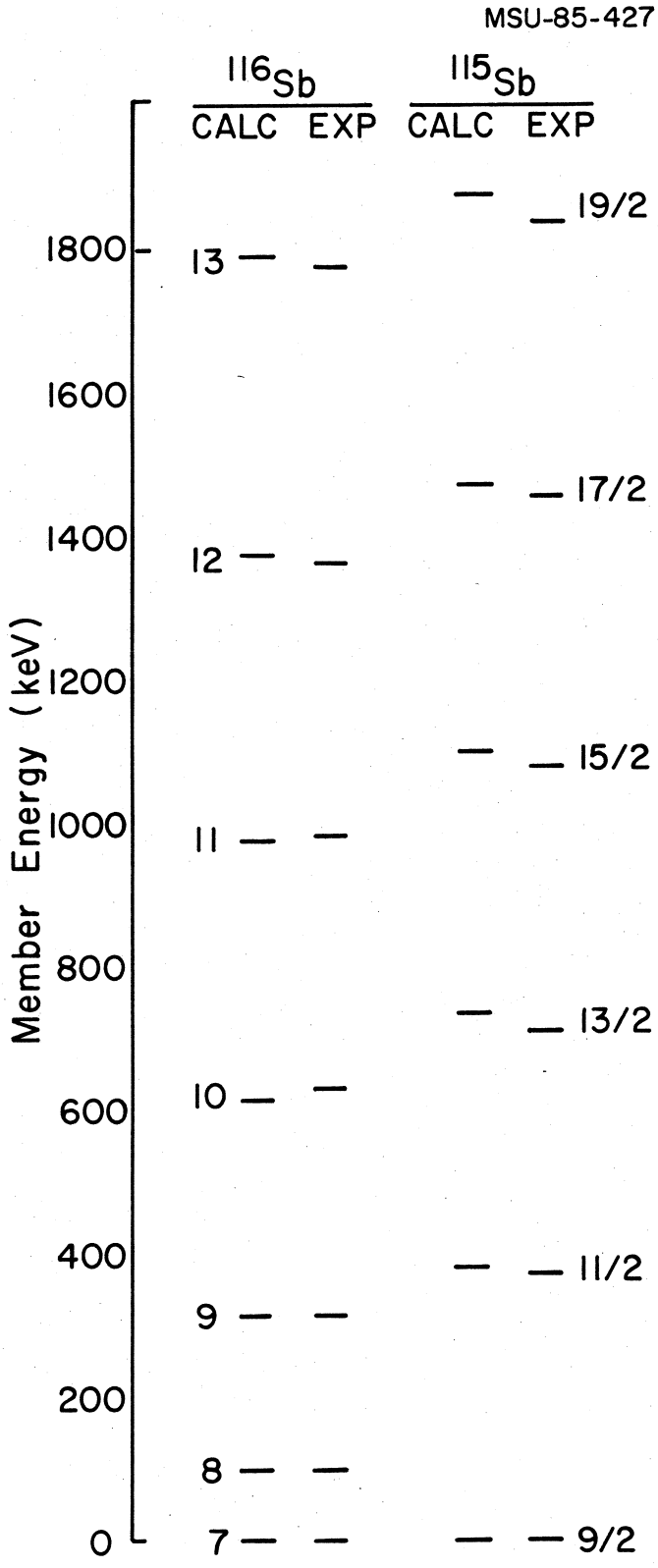
MSU-85-427
116Sb
CALC EXP
115Sb
CALC EXP
Member Energy (keV)
1800
1600
1400
1200
1000
800
600
400
200
0
13
12
11
10
9
8
7
19/2
17/2
15/2
13/2
11/2
9/2

Fig. 8